# Photoreversible Growth of Micropattern

Honghao Hou, Xiaodong Ma, Hongjie Xu, Zixing Shi, Jie Yin, and Xuesong Jiang*

**Self-organized surface patterns from the nano- to microscale inspired by nature find wide applications in functional intelligent materials in various fields. In particular, complex patterns with the reversible topographies that do not alter the material's intrinsic properties allow for the possibility of on-demand control of the surface properties. Herein, a facile strategy is presented to fabricate a micro/nanopatterned surface whose morphology can be changed timely and spatially by light. The complex pattern is fabricated on the surface of a photocuring coating through a one-step, self-patterned process, in which self-assembly of fluorinated azobenzene-containing polymer and photoreversible isomerization lead to the generation of compressive stress, resulting in the formation of a reversible surface pattern. The reversible change of the pattern morphology allows for light control of the adhesion and wettability of the surface. Moreover, the one-step approach to fabricate the complex pattern possesses characteristics similar to the formation process of the self-organizing micro/nanopatterns in nature. The feasibility and generality of this approach for obtaining such bioinspired, photoreversible, and self-organized patterned surfaces will find wide applications in functional intelligent materials with properties that can be tuned on-demand without altering the material's intrinsic properties.**

## 1. Introduction

As demonstrated by nature, self-organized surface patterns from the nano- to microscale can endow living creatures with certain types of special properties, such as self-cleaning effects,[1–4] antireflectivity,[3,5–9] controlled adhesion and release,[10–12] and the ability to capture water from fog.[13–15] For example, geckos and some insects can control surface adhesion because of the complex micro- and nanofibrillar arrays on their legs.[16–18] Inspired by these surface patterns and the interesting functions that are observed in nature, researchers have developed two common methods to fabricate structured surface patterns: top-down and bottom-up methods,[19,20] such as lithography, replica moulding, and self-organization. In biological systems, a bottom-up strategy has been adopted to hierarchically structure molecules to meter-scale biological organisms. Among these bottom-up techniques, surface pattern of a thin film is widely used to fabricate complex patterns on the surface, which usually involves compressive stress caused by the modulus mismatch between the surface and the bulk of the materials. Moreover, the resulting complex pattern on the artificial materials exhibits characteristics similar to the surface pattern in biology, such as papilla of the lotus and the venation network pattern of a leaf.[4,21] The ability to reversibly change complex pattern morphology is another important and interesting issue because it allows for the possibility to control the surface properties on-demand.[10–12,22] Octopus and cuttlefish are excellent examples in that they can rapidly switch their skin texture from smooth to complex 3D protuberances, or papillae, to camouflage themselves.[23–26] The bottom-up strategy usually involves fewer fabricating steps than does the up-down strategy, which leads to a short fabrication time, low cost, and consequently increased convenience.[19,20] However, there are few reports on using the bottom-up strategy to fabricate the micro/nanopattern surface.

In this paper, we present a facile bionic bottom-up strategy to fabricate a micropatterned surface, whose morphology can be changed timely and spatially by light. The complex micro/nanopattern was fabricated on the surface of a photocuring coating through a one-step, self-organized patterned process, in which the self-assembly of fluorinated azobenzene (AZO)-containing polymer and photoreversible isomerisation lead to the generation of compressive stress, resulting in the formation of a reversible surface pattern. The reversible change of the pattern morphology allows for light control of the adhesion and wettability of the surface. Light as a stimulus provides a facile approach to tune the surface features spatially and temporally and has some advantages over other stimuli, such as solvents,[27] temperature,[28] electrical field,[29] and mechanical force.[30–33] The light-control has been harnessed to obtain versatile micro/nanopatterns and structures such as wrinkle.[34–36] Moreover, it is well known that the gratings pattern generated by the polarized light illumination of AZO-containing polymers with the well-ordered arrangement of liquid crystal molecules[37–42] or the pattern of the multilayer systems containing

Dr. H. H. Hou, Dr. X. D. Ma, Prof. H. J. Xu,
Prof. Z. X. Shi, Prof. J. Yin, Prof. X. S. Jiang
School of Chemistry & Chemical Engineering
Shanghai Key Laboratory of Electrical Insulation and Thermal Ageing
State Key Laboratory for Metal Matrix Composite Materials
Shanghai Jiao Tong University
Shanghai 200240, P. R. China
E-mail: ponygle@sjtu.edu.cn

DOI: 10.1002/admi.201600528


© 2016 WILEY-VCH Verlag GmbH & Co. KGaA, Weinheim

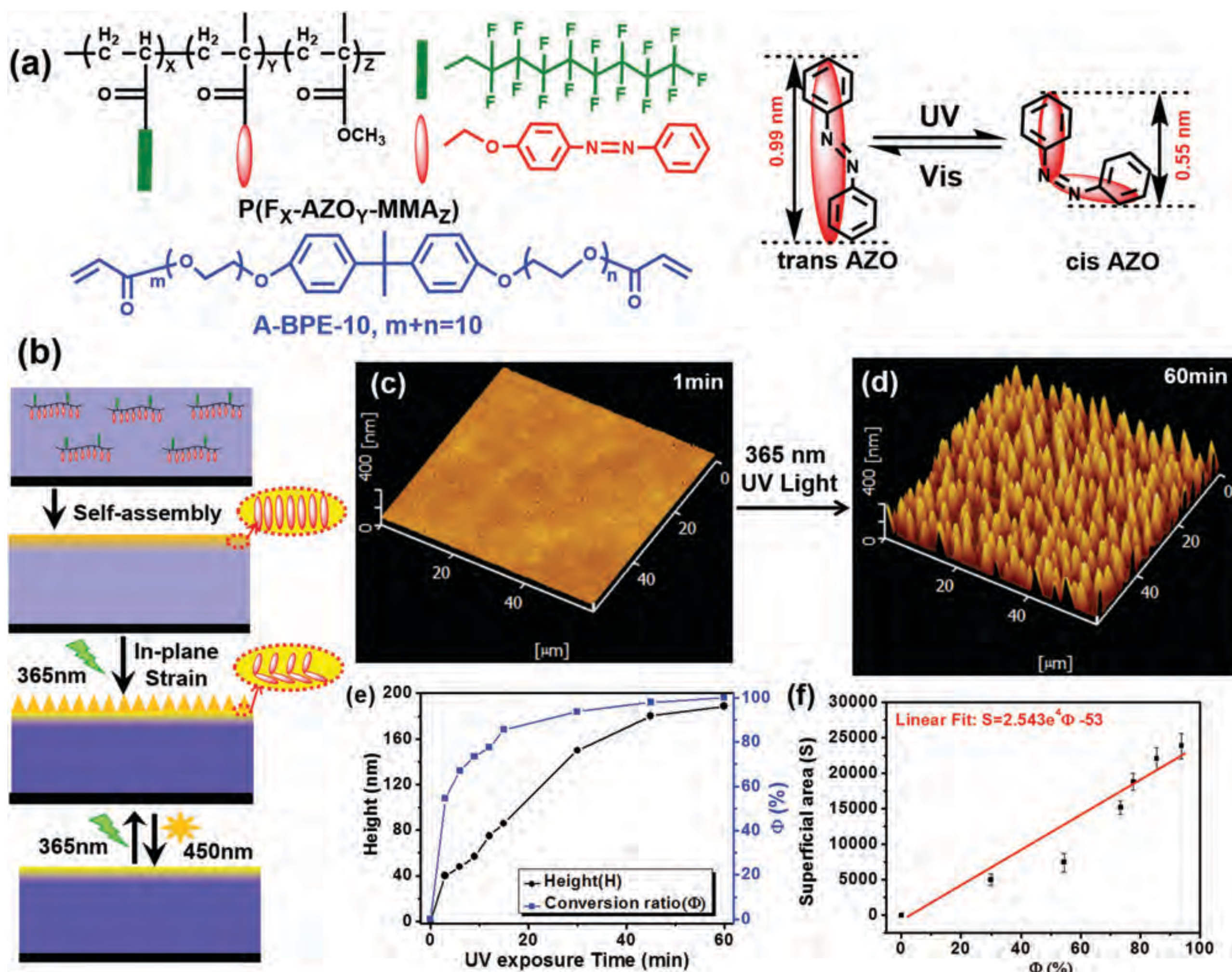


**Figure 1.** a) Chemical structure of fluorinated AZO copolymer P($F_X$-$AZO_Y$-$MMA_Z$) and schematic illustration showing the photoisomerization of AZO moiety. b) Strategy for the photoreversible, micropattern. c,d) 3D AFM images of photoreversible micropattern of P(F-$AZO_8$-MMA)/A-BPE-10 film under 365 nm UV irradiation for 1 min and 60 min, respectively. e) The characteristic height (H) of surface micro/nanopatterns and the photoisomerization conversion ratio (Φ) of AZO moiety in the micro/nanopatterned P(F-$AZO_8$-MMA)/A-BPE-10 films as a function of UV exposure time. For the convenience of statistical calculation, the photostationary state after sufficient UV exposure time at 365 nm is regarded as the complete photoisomerization state. f) The superficial area (S) as a function of the photoisomerization conversion ratio (Φ) of the AZO moiety of the surface pattern P(F-$AZO_8$-MMA)/A-BPE-10 films with different UV exposure times. The concentration of P(F-$AZO_8$-MMA) is 2 wt%.

AZO molecules with photo illumination using the top-down methods.[43,44] Yet the photoreversible microsurface pattern applying the biomimetic bottom-up method is rarely reported. Our one-step approach of micropattern to fabricate complex patterns possesses characteristics similar to the formation process of the self-organizing micro/nanopattern of biology in nature.

## 2. Results and Discussion

### 2.1. Photoinduced Growth of the Micropattern

The entire strategy to fabricate the photoreversible micropattern is illustrated in **Figure 1**. AZO-containing fluorinated polymer can self-assemble to form the top layer at the air/monomer liquid interface because of its low surface energy and vertical phase separation of fluorinated carbon chains. Upon exposure to 365 nm UV light, the conventional radical polymerization takes place in the bulk layer, whereas the photoisomerization of AZO moieties from *trans* to *cis* occurs in the top layer. The different volumetric changes between the top and bulk layers can cause compressive stress, resulting in the simultaneous formation of a surface pattern. Because of the well-known reversible photoisomerization of AZO, the morphology of the surface pattern is expected to be tunable with light. In our typical experiments, P(F-$AZO_8$-MMA) and the bifunctional acrylate A-BPE-10 are chosen as the AZO-containing fluorinated copolymer and the photocurable monomer, respectively. The chemical structures and detailed synthesis and characterization of these materials can be found in the Supporting Information (Figures S1–S4 and Table S1). A photocurable mixture of A-BPE-10 and P(F-$AZO_8$-MMA) (2 wt%) with a trace amount of photoinitiator I907 was drop-coated onto the glass slide

 © 2016 WILEY-VCH Verlag GmbH & Co. KGaA, Weinheim 

substrate. The surface pattern with lanky mastoid-shape features was observed by AFM(Atomic Force Microscope) on the surface of the cured film after irradiation with 365 nm UV light for 60 min under $N_2$ protection (Figure 1d), suggesting the feasibility of the strategy illustrated in Figure 1b. Note that our micropattern is quite different from the gratings pattern generated by the polarized light illumination of AZO-containing polymers with the well-ordered arrangement of liquid crystal molecules[37–42] or micro/nanopattern of multilayer systems containing AZO moieties using the top-down methods.[43,44] The AZO-containing fluorinated polymer P(F-$AZO_8$-MMA) is the key component in our strategy, which involves the formation of a top layer through the interfacial self-assembly and photoisomerization of AZO moieties.

The self-assembly of P(F-$AZO_8$-MMA) at the air/monomer liquid interface to form the top layer was confirmed by X-ray photoelectron spectroscopy (XPS). The strong signal related to F 1s was found in the XPS spectrum of the cured film's surface. The fluorine content of the surface is close to that of P(F-$AZO_8$-MMA) (Figure S5, Supporting Information), indicating that the surface should be completely covered by P(F-$AZO_8$-MMA). A control experiment was conducted to further understand the function of P(F-$AZO_8$-MMA) on the surface pattern. Instead of P(F-$AZO_8$-MMA), the AZO-containing copolymer P($AZO_8$-$MMA_2$) without fluorocarbon chains was added to the mixture of photocurable resin. No obvious surface pattern on the surface of the cured film with P($AZO_8$-$MMA_2$) was observed in the AFM image (Figure S6, Supporting Information), suggesting that the fluorocarbon chains are necessary for the generation of the surface pattern. Generally, creating the double layer is one of the key steps in forming the surface pattern. Because there are no fluorocarbon chains of low surface energy, P($AZO_8$-$MMA_2$) cannot self-assemble at the air/liquid interface to form the top layer, resulting in no formation of the surface pattern.

To obtain detailed insights into the formation behavior of the micropattern, we used AFM to trace the surface morphology dependence on irradiation time and used UV–vis spectra and real-time Fourier transform infrared (FTIR) to trace the kinetics of AZO's photoisomerization and photocrosslinking of A-BPE-10, respectively. The photocrosslinking of A-BPE-10 in the bulk layer is very fast and was nearly complete in 1 min under UV irradiation (Figure S7, Supporting Information). Compared to the fast photocrosslinking of A-BPE-10, the photoisomerization of AZO from the *trans* to *cis* state is much slower, and the photostationary state was reached in 60 min by UV irradiation (Figure S8, Supporting Information). After irradiation by UV light for 1 min, the surface of the cured film was quite smooth, and no pattern was observed by AFM (Figure 1c and Figure S10, Supporting Information). This result suggests that the micropattern was not caused by the photocrosslinking of A-BPE-10. Because of the low density of the C=C double bond in A-BPE-10, the photocrosslinking of A-BPE-10 in the bulk layer cannot lead to enough compressive stress to trigger the formation of the pattern. The surface pattern became obvious with increasing UV irradiation time, and the bamboo shoot-shaped bulge with a height of 200 nm was revealed by AFM after UV irradiation for 60 min. The statistical characteristic height (H) of the micropattern determined by AFM line analysis, and photoisomerization conversion ratio ($\Phi$) of the AZO moiety increased with the increasing UV irradiation time (Figure 1e and Figure S10, Supporting Information). Based on the AFM, UV–vis, and RT-FTIR results, we proposed that photo-induced *trans* to *cis* transition of AZO moieties of P(F-$AZO_8$-MMA) in the top layer leads to the generation of a micropattern. The *trans* isomer of AZO, with its straight rod-like shape, tends to align itself along the direction of and can tightly pack with vertical stretched structures in the plane. However, the *cis* isomer, with a curved shape, is less regular and cannot pack as closely as the *trans* isomer. The configuration transformation of P(F-$AZO_8$-MMA) from the *trans* to *cis* form under UV irradiation requires more space, resulting in the expansion of the top layer. The mismatch of the volume change between the top layer and the bulk layer leads to compressive stress, resulting in the generation of surface pattern. Upon visible light illumination, the surface pattern vanishes as AZO isomerizes from the *cis* to the *trans* form. Therefore, it is the photoreversible isomerization of AZO on the molecular scale that leads to the reversible surface pattern on the microscale.

### 2.2. Photoreversible Micropattern

Because the isomerization process of the AZO group is photoreversible, the limited space would be released with the photoisomerization from the crooked and noncompact *cis* form to the tightly packed *trans* form. It is expected that if the cured A-BPE-10 film irradiated by 365 nm UV light was subsequently exposed to 450 nm visible light irradiation, the size of the micro/nanopatterns of the patterned film would decrease with the photoisomerization process. Therefore, irradiation with UV light will generate surface pattern, whereas visible light will erase the micro/nanopattern. Indeed, the as-prepared film with the micro/nanopattern exhibits a photoreversible morphology (**Figure 2**). The corresponding morphology of the film surface with alternate irradiation of UV and visible light was monitored by AFM (Figure 2a–e). The height (H) and root mean square surface roughness (RMS roughness) of the film surface micro/nanopatterns were determined by AFM line analysis (Figure 2f). As revealed in Figure 2, when the as-prepared micro/nanopatterned A-BPE-10 film exposed to 365 nm UV light for 30 min was subsequently exposed to 450 nm visible light for 6 h, the height of the film micro/nanopatterns decreased from 150 nm to ≈60 nm, accompanied by a sharp decline in the RMS surface roughness. Interestingly, after 12 h of visible light irradiation, the micro/nanopatterns disappeared and the film surface became almost plain, with a large decrease in the surface RMS roughness to a very low value. Because of the release of extrusion stress with the photoisomerization process from the crooked and noncompact *cis* form to the tightly packed *trans* form upon 450 nm visible light exposure, the ordered configuration of the AZO moiety on the top layer of the film required less space and the protuberance micro/nanopattern was relaxed. The generation and disappearance of micro/nanopatterns is determined by the molecule structure deflection of the AZO moiety in the top layer of the film as a result of the photoisomerization of the AZO groups under light irradiation. It is remarkable that the patterned film can undergo photoreversible morphology


© 2016 WILEY-VCH Verlag GmbH & Co. KGaA, Weinheim

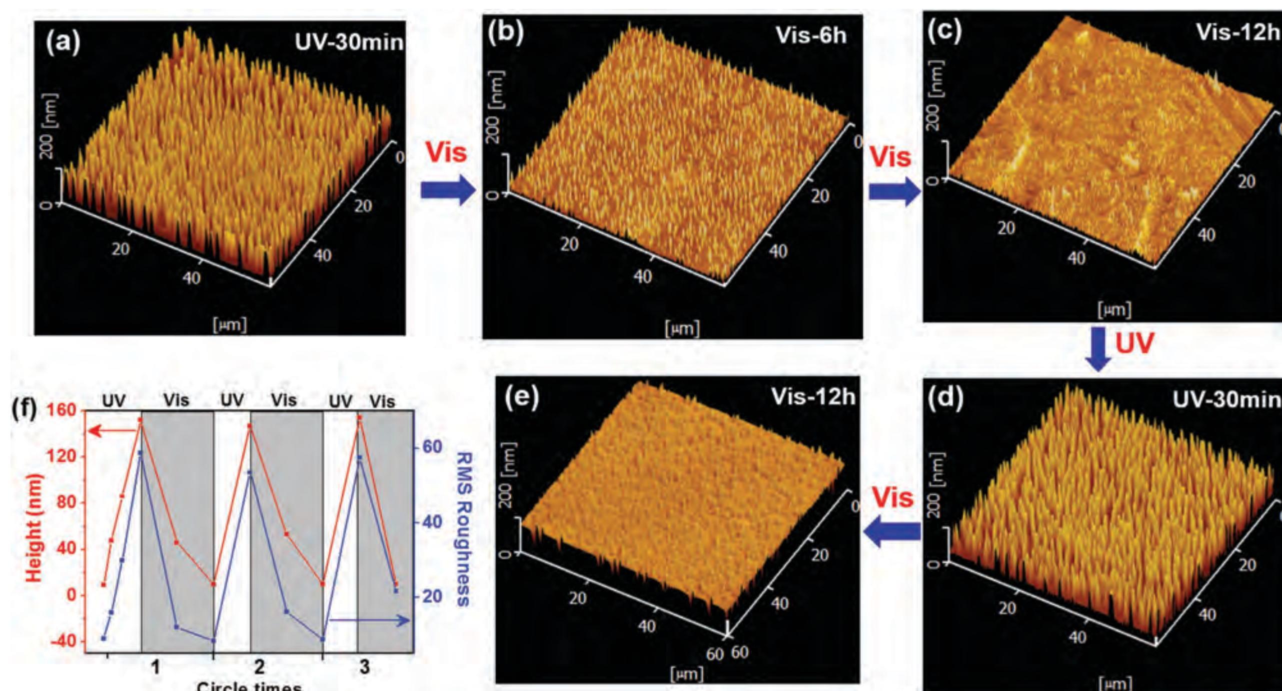


**Figure 2.** a–e) 3D AFM images and f) their corresponding height and RMS surface roughness showing the tunable morphology of micropattern P(F-AZO$_8$-MMA)/A-BPE-10 films with sequential, cyclic photocontrol using 365 nm UV light followed by 450 nm visible light irradiation. a–e) The inset text shows the illumination type and corresponding irradiation time. f) The top axis text shows the illumination type. UV represents for 365 nm UV light, VIS represents 450 nm visible light. The white and gray regions represent 365 nm UV light exposure and 450 nm visible light irradiation, respectively.

from surface pattern to a plane film for more than three cycles (Figure 2). This result indicates that the micro/nanopatterns were erased and recovered circularly upon light irra diation of different dimensions, also suggesting the feasibility of the photoreversible micro/nanopattern.

As for our gradient bilayer system prepared by the self-assembly of fluorinated polymer at the air/liquid interface, topographic transition resulting from the surface instability response to external stimulate is indeed a controlled, reversible surface roughening transition. We purposed this surface instability-induced micropattern as a special “wrinkle” pattern whose dynamical growth of the micropattern develops from the initial nonperiodic, nucleation-like, isolated features to the final periodic continuous architecture. The surface micropattern can be described by a sinusoidal vertical deflection of the film

$$y = A\sin\left(\frac{2\pi}{\lambda}\cdot x\right) \tag{1}$$

where D and H are the characteristic dimension and height (peak to valley) of the sinusoidal micro/nanopatterns, respectively.

The superficial area of the top layer (S) of sinusoid-shaped micro/nanopatterns in one period is equal to the indefinite integral of the sinusoid function in the interval of one dimension (D)

$$S = \int_0^D y\,dx \tag{2}$$

Substituting Equation (1) into Equation (2) yields

$$S = \int_0^D A\sin\left(\frac{2\pi x}{\lambda}\right)dx = -\frac{A}{2\omega}\left(\cos\frac{\lambda\omega}{2} - \cos 0\right) \tag{3}$$

Because D• $\omega = 2\pi$, $\cos\pi = -1$ and $\cos 0 = 1$, the following equation is obtained

$$S = \frac{A\lambda}{2\pi} \tag{4}$$

Regardless of the extremely small change in thickness before and after irradiation, the superficial area (S) of the micro/nanopattern represents the volume change of micro/nanopattern fluctuation in the horizontal plane. In our photoreversible, micropattern system, the volume change of AZO molecules induced by the configuration transformation of P(F-AZO$_8$-MMA) results in the extrusion to neighbors and the protrusion micro/nanopattern, which is responsible for the morphology transition of the film surface. In other words, the volume change of the sinusoid micro/nanopatterns (superficial area, S) is dependent on the molecular volume change of the AZO moiety (ΔS). Herein, we defined a constant K as the correlation coefficient between the superficial area (S) of the micro/nanopattern and the volume change of the AZO moiety (ΔS), giving Equation (5)

$$S = K^*\Delta S^*\Phi \tag{5}$$

 © 2016 WILEY-VCH Verlag GmbH & Co. KGaA, Weinheim 

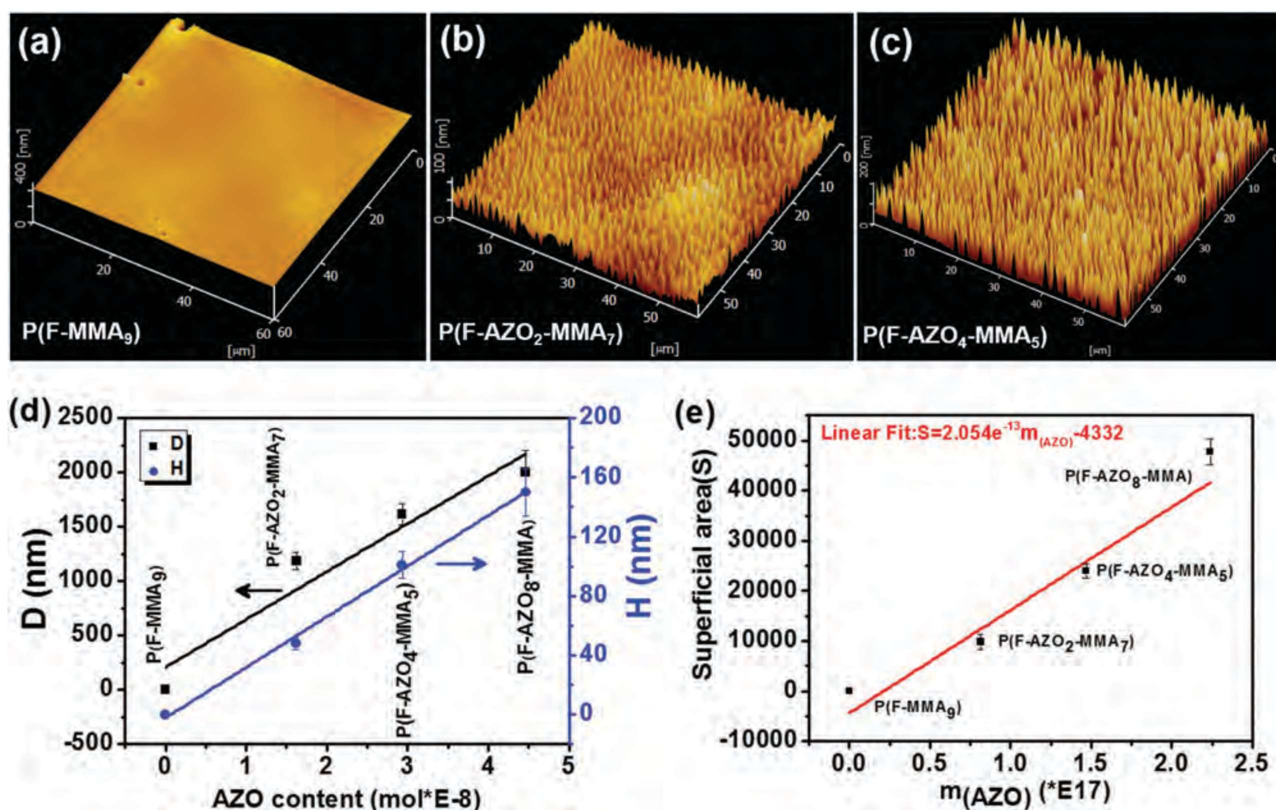


**Figure 3.** a–c) 3D AFM images of the surface pattern cured A-BPE-10 films fabricated under 365 nm UV irradiation for 60 min with different fluorinated AZO copolymers: (a) P(F-MMA$_9$), (b) P(F-AZO$_2$-MMA$_7$), (c) P(F-AZO$_4$-MMA$_5$). d) Dimension (D, left vertical axis) and height (H, right vertical axis) of the surface pattern cured A-BPE-10 films as a function of AZO content of different fluorinated AZO copolymers: P(F-MMA$_9$), P(F-AZO$_2$-MMA$_7$), P(F-AZO$_4$-MMA$_5$), P(F-AZO$_8$-MMA). e) The superficial area (S) of the surface pattern film as a function of the amount ($m_{(AZO)}$) of azobenzene moieties in different fluorinated AZO copolymers. The concentration of all the fluorinated polymers is fixed at 2 wt%, and the surface pattern cured A-BPE-10 films were fabricated under 365 nm UV irradiation for 60 min.

The molecular volume (superficial area) change induced by the AZO isomerization ($\Delta S$) can be calculated by Equation (6)

$$\Delta S = m_{(AZO)} * \Delta S_{min} \quad (6)$$

where $m_{(AZO)}$ represents the amount of azobenzene moieties and $\Delta S_{min}$ represents the volume change of one azobenzene molecule between the *trans* and *cis* state. According to the calculation of density functional theory (DFT), $\Delta S_{min}$ is ≈0.12 nm$^3$ (Figure S12, Supporting Information), which complies with previous theoretical results.[45]

Combining Equations (4)–(6) yields Equation (7), which quantifies the relationship between the microscopic micro/nanopattern and molecular volume change of AZO

$$S = \frac{A\lambda}{2\pi} = K * m_{(AZO)} * \Delta S_{min} * \Phi \quad (7)$$

where $\Phi$ represents the photoisomerization conversion ratio of the AZO moiety in the top layer of the surface pattern film. According to Equation (7), it is assumed that the superficial area of the surface pattern film (S) is linearly dependent on the amount of AZO (m) and its photoisomerization conversion. This assumption is proven in Figure 1f, which presents a good linear relationship between S and AZO conversion from the *trans* to *cis* form ($\Phi$), from which the coefficient K can be calculated as $1.71 \times 10^{-12}$. Our gradient bilayers system may have a little bad effect on the perfect linear relationship between S and $\Phi$. To fix the concentration of the fluorinated polymer (2 wt%) and the UV light exposure time (60 min, conversion of *trans* to *cis* is nearly 100%), we also prepared a series of surface patterns using fluorinated polymers with different AZO moiety contents (**Figure 3**). The characteristic H and D of the resulting surface pattern were determined by AFM analysis (Figure 3e and Figure S13, Supporting Information). The superficial area (S) of the surface pattern film increases linearly with the AZO content ($m_{(AZO)}$) in ifferent fluorinated AZO copolymers, from which the coefficient K was calculated as $1.71 \times 10^{-12}$ (Figure 3e). Nearly the almost same value of coefficient K from two independent series of experiments suggests the feasibility of Equation (7) and confirms that the driving force of the surface pattern is the molecular volume change induced by AZO photoisomerization.

Furthermore, by varying the concentration of the fluorinated copolymer P(F-AZO$_8$-MMA), a series of surface patterns was prepared, and the characteristic D and A values were determined by AFM analysis (**Figure 4** and Figure S14, Supporting Information). A good linear relationship between the


© 2016 WILEY-VCH Verlag GmbH & Co. KGaA, Weinheim

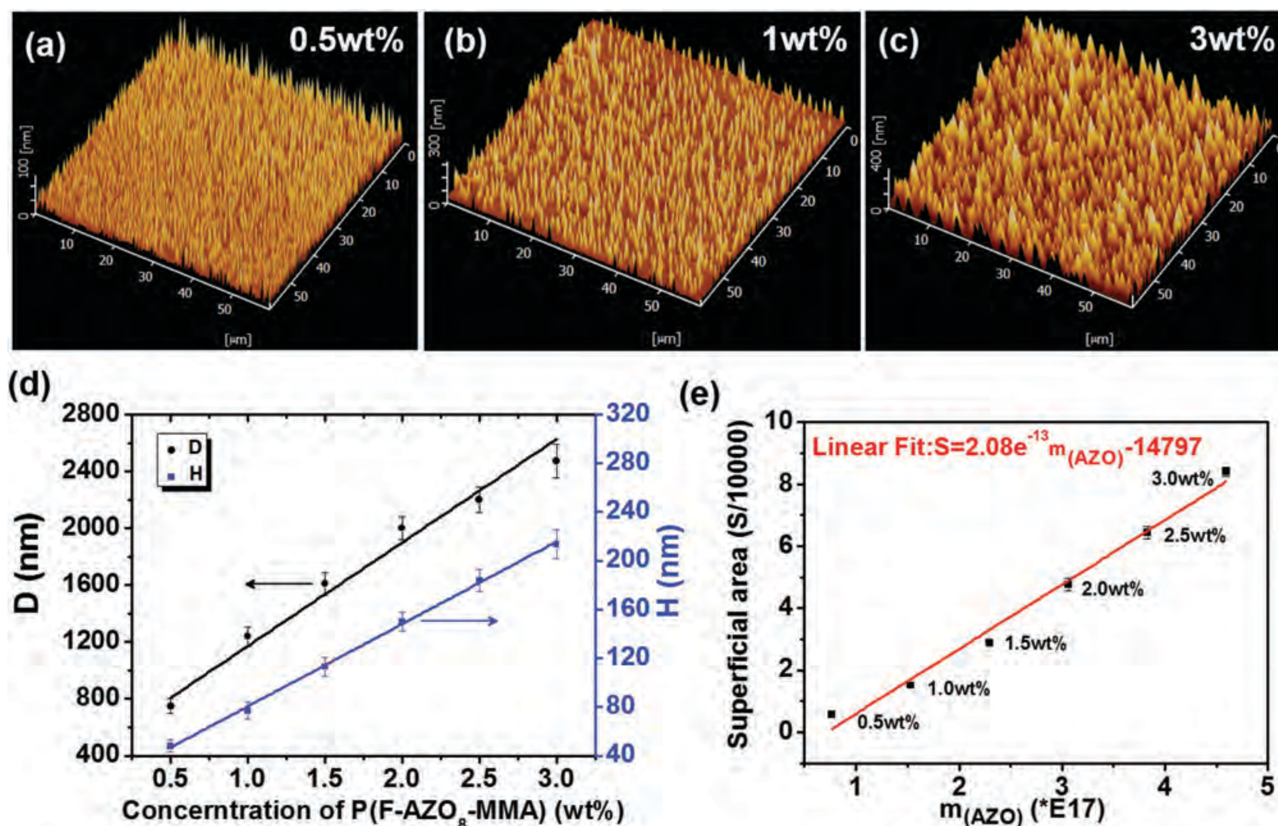


**Figure 4.** a–c) Typical 3D AFM images of the surface pattern of cured A-BPE-10 films fabricated under 365 nm UV irradiation for 30 min within different concentration of copolymer P(F-$AZO_8$-MMA): a) 0.5 wt%, b) 1 wt%, c) 3 wt%, respectively. d) Dimension (D, left vertical axis) and height (H, right vertical axis) of the surface pattern cured A-BPE-10 films fabricated under 365 nm UV irradiation for 30 min within different concentration of copolymer P(F-$AZO_8$-MMA). e) The superficial area (s) of the micro/nanopatterned film as a function of the amount ($m_{(AZO)}$) of AZO moiety within different concentration of copolymer P(F-$AZO_8$-MMA).

characteristic D and A values of the surface patterns and the concentration of P(F-$AZO_8$-MMA) was obtained, revealing that the obtained surface patterns in our system are controlled and conform to the linear buckling theory for our typical gradient bilayer system (see Section 4.9, Supporting Information).

The stability of the micropattern in the dark is demonstrated since AZO compounds show also a thermal isomerization. As depicted in **Figure 5**, the micro/nanopattern did not remarkably change after kept at room temperature in the dark for more than one month, and the height of micro/nanopattern decreased ≈20 nm for kept in the dark at 70 °C for more than 72 h. Apparently, the micropattern exhibit a relatively long-term thermostability. Also, to verify the feasibility of the photoreversible, micropattern, we chose P($F_2$-$AZO_8$) as the fluorinated

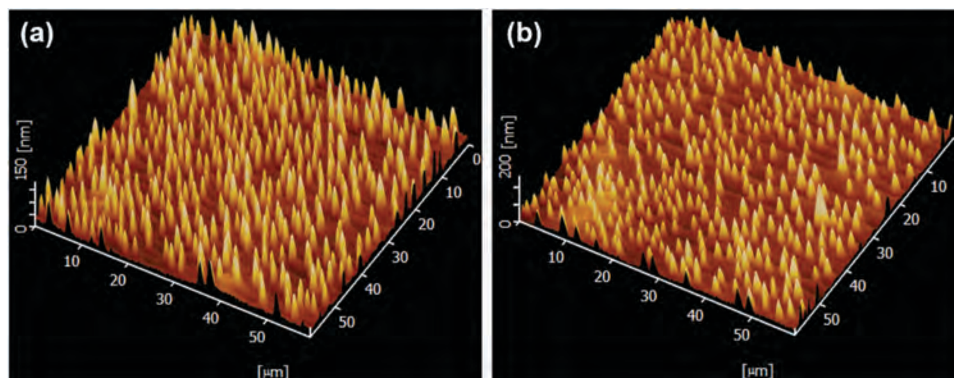


**Figure 5.** 3D AFM images showing the stability of phototunable morphology of micropattern P(F-$AZO_8$-MMA)/A-BPE-10 films: a,b) using 365 nm UV light irradiation for 60 min followed by (a) kept at 70 °C in the dark for more than 72 h or b) at room temperature for more than one month. The curing condition is the same as before.


© 2016 WILEY-VCH Verlag GmbH & Co. KGaA, Weinheim

AZO copolymer and PEGDA as the photocurable resin to fabricate the surface pattern. Similar to the results of the P(F-AZO$_8$-MMA)/A-BPE-10 system, the tip-island surface pattern was generated by 365 nm UV light exposure for 30 min, followed by the surface gradually becoming flat upon 450 nm visible light illumination (Figure S11, Supporting Information). After 4 h of 450 nm visible light illumination, the original surface pattern with a height of 250 nm and a dimension of 800–1000 nm was nearly flat and micro/nanopattern-free.

To verify the feasibility of our strategy, we replaced the monomer A-BPE-10 with three other types of common multiacrylate monomers as photocrosslinkers: polyethylene glycol diacrylate (PEGDA), poly(propylene glycol) diacrylate (PPGDA), and 1,6-hexanediol diacrylate (HDDA). Similar to the system of A-BPE-10, the micro/nanopatterns can be found in different photocuring systems using other photocrosslinkers (Figure S15, Supporting Information). Additionally, to further verify the mechanism of the micropattern, we designed and synthesized a type of reactive fluorinated AZO copolymer, F-AZO$_8$-EMA, with a residue double bond (Figure S16, Supporting Information). Instead of P(F-AZO$_8$-MMA), the formation of the micropattern can also be realized by P(F-AZO$_8$-EMA). In this homogeneous photocuring system of reactive fluorinated AZO copolymer, P(F-AZO$_8$-EMA) participates in the photocrosslinking reaction with A-BPE-10 monomer, both of which become the moieties of the monolithic film upon UV light exposure as the fabrication of the micro/nanopatterns is initiated. Therefore, we can further exclude the possible mechanism of kinetically trapped phase separation.

### 2.3. Phototunable Surface Properties

Surfaces patterned with micro- or nanoscale features offer a new type of smart materials that can change their physical properties, e.g., surfaces with tunable adhesion and friction, by dynamically tuning surface geometry in response to external stimuli without altering the bulk properties.[8] Because of the large change in surface morphology and roughness of our photoreversible surface pattern before and after photo-erasure, if the light is controlled in sequence, the surface morphology can be reversibly tuned from patterned, vertically aligned tip-island macro- and nanopatterns, to an unpatterned, nearly planar surface, resulting in dramatic and reversible surface properties.

First, the adhesion and friction forces of the surface pattern films were measured through the colloidal probe AFM, the resolution and sufficient contact area of which are required to study surface interactions on the micro- and nanoscale.[46–48] The experimental value of the pull-off force was extracted from the minimum of the retraction curves and was taken as the adhesion force.[46–48] The characteristic force–displacement curves of the patterned surface and the nonmicro/nanopattern plane surface photoerasure from the surface pattern were obtained (Figure S17, Supporting Information). The film with the surface pattern fabricated under UV exposure for 30 min showed a clear pull-off event of the patterned film and an adhesive force of 180 nN (red line). When the film was sequentially illuminated by visible light of 450 nm for 12 h, a clear drop in the pull-off force was observed (95 nN, black line). This result indicates that the film presents a decrease of adhesion force when the surface morphology varies from surface pattern to unpatterned. Given our current materials system, the enhancement of adhesion is limited because of the hydrophily and adherence of the base A-BPE-10 resins. The change of the surface morphology also affected the slope of the loading curve, which reflects the effective Young's modulus of the patterned surface. The slope of the loading curve of the unpatterned surface film was slightly smaller, indicating that the macro and nano patterns could be helpful to increase the surface rigidity. Therefore, when the patterns of the surface were photo-wiped via visible light illumination, the surface appeared softer. However, the nature of the identical materials in the two films determines the limit of the drop in surface rigidity. With the appropriate choice of materials, our general fabrication strategy can be extended to generating smaller dimension structures to provide even greater enhancement. The adhesive and nonadhesive states were reversibly cycled by switching the light exposure (**Figure 6**a), demonstrating the first case of photoreversible adhesion. Note that the adhesion force of micro/nanopattern can be switched for more than six cycles, in which the adhesion force does not significantly fluctuate. Additionally, as a reference, we prepared a pure P(F-AZO$_8$-MMA) film spin-coated

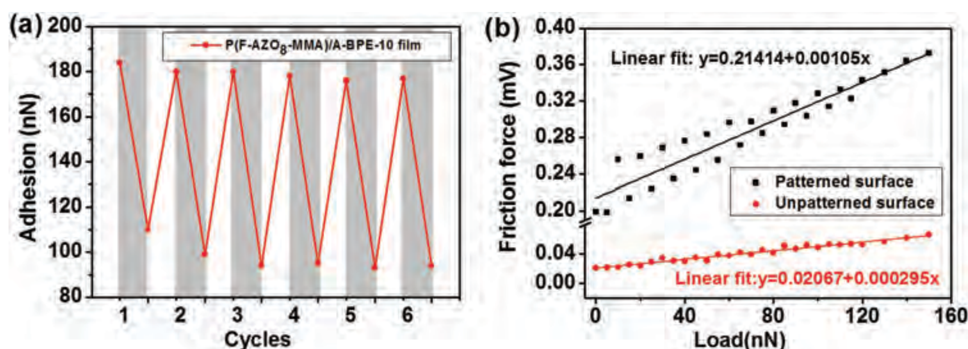


**Figure 6.** a) Changes in the adhesion force measured on the P(F-AZO$_8$-MMA)/A-BPE-10 film (black quadrate) with the cyclic, sequential photocontrol of 365 nm UV and 450 nm visible light irradiation. The white and grey regions represent 365 nm UV light and 450 nm visible light, respectively. b) The friction force signal detected by AFM friction force mode (FFM) of patterned surfaces and unpatterned surfaces as a function of the preload. Patterned surface of P(F-AZO8-MMA)/A-BPE-10 film was fabricated by irradiation under 365 nm UV light for 30 min. Followed by the irradiation of 450 nm visible light for 12 h, the micro/nanopattern was erased to generate the unpatterned surface.


© 2016 WILEY-VCH Verlag GmbH & Co. KGaA, Weinheim

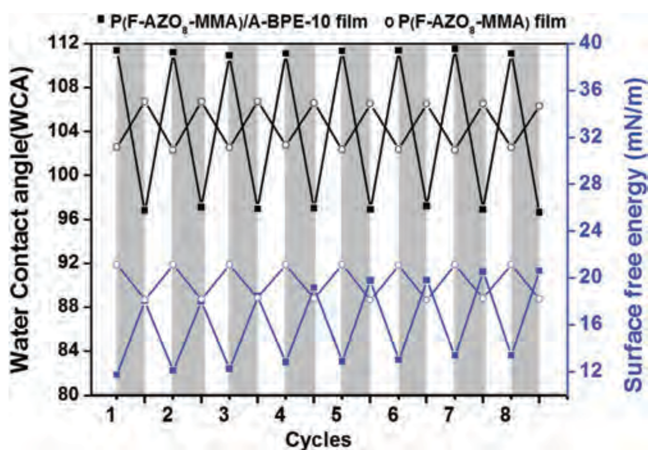


**Figure 7.** Changes in water contact angle (WCA, black line, left vertical axis) and surface free energy(blue line, right vertical axis) of the surface pattern P(F-AZO8-MMA)/A-BPE-10 film (solid black quadrate)with pure P(F-AZO$_8$-MMA) copolymer reference film (empty circle) with cyclic, sequential photocontrol with 365 nm UV and 450 nm visible light irradiation. The white and gray regions represent 365 nm UV light exposure and 450 nm visible light irradiation, respectively.

onto glass substrate and verified the reversibility of its adhesion force during sequential UV and visible light exposure for six cycles (Figure S17b, Supporting Information). The photoreversible change value of the adhesion force (≈15 nN) was much lower than that of the surface pattern A-BPE-10 film (≈75 nN), suggesting that photo-isomerization of the AZO moiety plays a nondominant role in the surface properties. The change in the surface morphology makes a significant difference in the surface adhesion properties. The friction property of the micro/nanopatterned surface and unpatterned surface was demonstrated in Figure 6b. The friction factor for the micro/nanopatterned surface is $1.05 \times 10^{-3}$, which is much higher than that of the smooth surface ($2.95 \times 10^{-4}$, red line in Figure 6b). These properties are switchable upon the photocontrol process of the surface pattern. Moreover, the photoactuated switching of the surface properties between adhesive (rough) and nonadhesive (smooth) states also demonstrates that the reversibility of the micro/nano patterned surface can be achieved.

Furthermore, the wettability properties of the photoreversible, micropatterned surface were also investigated via contact angle measurements. **Figure 7** presents the changes in water contact angle (WCA) and surface free energy of the P(F-AZO$_8$-MMA)/A-BPE-10 micro/nanopatterned film as well as the pure P(F-AZO$_8$-MMA) copolymer film as a reference at various stages of UV and visible irradiation over eight cycles. The WCA of the micro/nanopatterned surface after UV irradiation was ≈112° (Figure S18a, Supporting Information). The relatively large CA could be attributed to the low surface energy caused by the J-aggregates of the fluorine groups on the surface of the films. After irradiation by visible light, the surface pattern disappeared, and the average CA decreased to ≈95° (Figure S18b, Supporting Information). Note that this contact angle change is nearly completely reversible after UV light irradiation. The wettability of the photoreversible patterned surface can be reversibly tuned under the external stimulus of light. The wettability of the pure P(F-AZO$_8$-MMA) copolymer reference film also underwent a reversible change at a lower value of 6°CA compared to that of the surface pattern A-BPE-10 film (20°), which agrees with previous works.[49–53] Note that the changes in contact angle and surface free energy of the fluorine-containing azobenzene polymer film are distinctly different from those of our photoreversible surface pattern film. With UV irradiation of fluorine-containing azobenzene polymer films, the *trans* isomers photoswitch to *cis* isomers of azobenzene, and the existing fluorine group has different dipole moments and a decrease in WCA.[48] However, the photoreversible surface pattern film undergoes an immense change in surface wettability and improvement of CA. It is well known that surface chemistry and morphology are the two key factors that govern the surface wettability.[54–57] The reversible wettability of the surface pattern surface is a result of both the surface microarchitecture and the existence of fluorine and AZO groups. Upon UV light exposure, gradual generation of the patterns leads to a large increase in surface roughness, which immensely changes the wettability of the surface and significantly improves the contact angle. The different dipole moments during the photoisomerization of azobenzene decrease the wettability and contact angle. Thus, the main cause of the increased contact angle and surface energy is the change in the morphology and surface roughness from the unpatterned plane surface to the micropatterned surface. The existence of fluorine and AZO groups resulting from the change of the dipole moments during the process of AZO photoisomerization plays an opposite and unfamiliar role in the enhancement of the wettability and surface free energy, which may explain the limited effect on the wettability of the photoreversible surface patterned surface.

## 3. Conclusions

A novel bottom-up strategy for obtaining a photoreversible micropattern was reported, which was fabricated by the mismatch of volume change between gradient bilayers as a result of the photoisomerization of azobenzene groups and the self-assembly of fluorinated azobenzene copolymer at the air/liquid resin interface. We demonstrated that the micro/nanopatterns undulated to accommodate the configuration transformation of AZO moieties under light-control. Under sequential UV and visible light exposure, the hierarchical film can reversibly achieve a change in its surface morphology from a micro- and nanosurface pattern to an unpatterned, flat surface. This topographical change, combined with the appropriate bioinspired adhesive design, allows for photoactuated switching of the surface properties between adhesive (rough) and nonadhesive (smooth) states. Aside from the tunable changes in adhesion properties, we expect the fabricated hierarchical substrates to exhibit unique friction and wetting properties. Such bioinspired, photoreversible micropatterned surfaces may find wide applications in functional intelligent materials with topographies and properties that can be tuned on-demand without altering the intrinsic properties of the materials.

## 4. Experimental Section

*Preparation of Photocured Coating Sample*: Acrylate monomer (1.0 g) and a trace amount of photoinitiator were dissolved in chloroform (1 mL)

 © 2016 WILEY-VCH Verlag GmbH & Co. KGaA, Weinheim 

by stirring. The as-prepared resin mixture with a fixed mass was drop-coated onto an infrared transmitting silicon wafer or a glass slide. The thickness was fixed at 200 μm. The sample was maintained at 60 °C for 30 min to remove the solvent and then photocured by irradiation with 365 nm UV light (using a light-emitting diode (LED) with an intensity of ≈10 mW $cm^{-2}$) for the desired time at nitrogen atmosphere.

## Supporting Information

Supporting Information is available from the Wiley Online Library or from the author.

## Acknowledgements

The authors thank the National Basic Research Program (2013CB834506), National Nature Science Foundation of China (21274088, 51373098, and 21522403) for their financial support.

Received: June 7, 2016
Revised: July 8, 2016
Published online:

[1] R. Blossey, *Nat. Mater.* **2003**, *2*, 301.
[2] W. R. Hansen, K. Autumn, *Proc. Natl. Acad. Sci. USA* **2005**, *102*, 385.
[3] W. L. Min, B. Jiang, P. Jiang, *Adv. Mater.* **2008**, *20*, 3914.
[4] S. G. Lee, H. S. Lim, D. Y. Lee, D. Kwak, K. Cho, *Adv. Func. Mater.* **2013**, *23*, 547.
[5] M. Ibn-Elhaj, M. Schadt, *Nature* **2001**, *410*, 796.
[6] J. A. Hiller, J. D. Mendelsohn, M. F. Rubner, *Nat. Mater.* **2002**, *1*, 59.
[7] C. Lee, S. Y. Bae, S. Mobasser, H. Manohara, *Nano Lett.* **2005**, *5*, 2438.
[8] J. Q. Xi, M. F. Schubert, J. K. Kim, E. F. Schubert, M. Chen, S. Y. Lin, W. Liu, J. A. Smart, *Nat. Photonics* **2007**, *1*, 176.
[9] H. K. Raut, V. A. Ganesh, A. S. Nair, S. Ramakrishna, *Energy Environ. Sci.* **2011**, *4*, 3779.
[10] E. P. Chan, E. J. Smith, R. C. Hayward, A. J. Crosby, *Adv. Mater.* **2008**, *20*, 711.
[11] Y. K. Lai, F. Pan, C. Xu, H. Fuchs, L. F. Chi, *Adv. Mater.* **2013**, *25*, 1682.
[12] D. M. Drotlef, P. Blumler, A. del Campo, *Adv. Mater.* **2014**, *26*, 775.
[13] A. R. Parker, C. R. Lawrence, *Nature* **2001**, *414*, 33.
[14] Y. Zheng, H. Bai, Z. Huang, X. Tian, F. Q. Nie, Y. Zhao, J. Zhai, L. Jiang, *Nature* **2010**, *463*, 640.
[15] K. Liu, X. Yao, L. Jiang, *Chem. Soc. Rev.* **2010**, *39*, 3240.
[16] K. Autumn, Y. A. Liang, S. T. Hsieh, W. Zesch, W. P. Chan, T. W. Kenny, R. Fearing, R. J. Full, *Nature* **2000**, *405*, 681.
[17] K. Autumn, M. Sitti, Y. A. Liang, A. M. Peattie, W. R. Hansen, S. Sponberg, T. W. Kenny, R. Fearing, J. N. Israelachvili, R. J. Full, *Proc. Natl. Acad. Sci. USA* **2002**, *99*, 12252.
[18] H. Lee, B. P. Lee, P. B. Messersmith, *Nature* **2007**, *448*, 338.
[19] A. del Campo, E. Arzt, *Chem. Rev.* **2008**, *108*, 911.
[20] A. Biswas, I. S. Bayer, A. S. Biris, T. Wang, E. Dervishi, F. Faupel, *Adv. Colloid Interface Sci.* **2012**, *170*, 2.
[21] P. Kim, M. Abkarian, H. A. Stone, *Nat. Mater.* **2011**, *10*, 952.
[22] E. Lee, M. Zhang, Y. Cho, Y. Cui, J. Van der Spiegel, N. Engheta, S. Yang, *Adv. Mater.* **2014**, *26*, 4127.
[23] J. J. Allen, G. R. Bell, A. M. Kuzirian, R. T. Hanlon, *J. Morphol.* **2013**, *274*, 645.
[24] E. J. Kelman, R. J. Baddeley, A. J. Shohet, D. Osorio, *Proc. R. Soc. London, Ser. B* **2007**, *274*, 1369.
[25] R. Hanlon, *Curr. Biol.* **2007**, *17*, R400.
[26] A. Barbosa, L. M. Mathger, C. Chubb, C. Florio, C. C. Chiao, R. T. Hanlon, *J. Exp.Biol.* **2007**, *210*, 1139.
[27] H. S. Kim, A. J. Crosby, *Adv. Mater.* **2011**, *23*, 4188.
[28] U. Manna, M. C. D. Carter, D. M. Lynn, *Adv. Mater.* **2013**, *25*, 3085.
[29] D. van den Ende, J. D. Kamminga, A. Boersma, T. Andritsch, P. G. Steeneken, *Adv. Mater.* **2013**, *25*, 3438.
[30] J. H. Lee, H. W. Ro, R. Huang, P. Lemaillet, T. A. Germer, C. L. Soles, C. M. Stafford, *Nano Lett.* **2012**, *12*, 5995.
[31] J. Yin, J. L. Yague, D. Eggenspieler, K. K. Gleason, M. C. Boyce, *Adv. Mater.* **2012**, *24*, 5441.
[32] J. Sharp, K. Thomas, M. Weir, *Phys. Rev. E* **2007**, *75*, 011601.
[33] D.-Y. Khang, J. A. Rogers, H. H. Lee, *Adv. Funct. Mater.* **2009**, *19*, 1526.
[34] D. Yang, L. H. He, *Smart Mater. Struct.* **2014**, *23*, 045012.
[35] T. Takeshima, W. Y. Liao, Y. Nagashima, K. Beppu, M. Hara, S. Nagano, T. Seki, *Macromolecules* **2015**, *48*, 6378.
[36] W. Wang, J. Lin, C. Cai, S. Lin, *Eur. Polym. J.* **2015**, *65*, 112.
[37] J. Kumar, L. Li, X. L. Jiang, D.-Y. Kim, T. S. Lee, S. Tripathy, *Appl. Phys. Lett.* **1998**, *72*, 2096.
[38] K. G. Yager, C. J. Barrett, *Curr. Opin. Solid State Mater. Sci.* **2001**, *5*, 487.
[39] A. Natansohn, P. Rochon, *Chem. Rev.* **2002**, *102*, 4139.
[40] C. Hubert, C. Fiorini-Debuisschert, I. Maurin, P. Raimond, *Adv. Mater.* **2002**, *14*, 729.
[41] K. G. Yager, C. J. Barrett, *J. Photochem. Photobiol., A* **2006**, *182*, 250.
[42] C. J. Barrett, J.-i. Mamiya, K. G. Yager, T. Ikeda, *Soft Matter* **2007**, *3*, 1249.
[43] C. Y. Zong, Y. Zhao, H. P. Ji, X. Han, J. X. Xie, J. J. Wang, Y. P. Cao, S. C. Jiang, C. H. Lu, *Angew. Chem.* **2016**, *128*, 3999.
[44] T. Takeshima, W. Liao, Y. Nagashima, K. Beppu, M. Hara, S. Nagano, T. Seki, *Macromolecules* **2015**, *48*, 6378.
[45] T. Naito, K. Horie, I. Mita, *Macromolecules* **1991**, *24*, 2907.
[46] E. Svetushkina, N. Puretskiy, L. Ionov, M. Stamm, A. Synytska, *Soft Matter* **2011**, *7*, 5691.
[47] J. Erath, S. Schmidt, A. Fery, *Soft Matter* **2010**, *6*, 1432.
[48] H.-J. Butt, B. Cappella, M. Kappl, *Surf. Sci. Rep.* **2005**, *59*, 1.
[49] W. Jiang, G. Wang, Y. He, X. Wang, Y. An, Y. Song, L. Jiang, *Chem. Commun.* **2005**, *28*, 3550.
[50] S.-K. Oh, M. Nakagawa, K. Ichimura, *J. Mater. Chem.* **2002**, *12*, 2262.
[51] C. L. Feng, Y. J. Zhang, J. Jin, Y. L. Song, L. Y. Xie, G. R. Qu, L. Jiang, D. B. Zhu, *Langmuir* **2001**, *17*, 4593.
[52] S. Abrakhi, S. Peralta, O. Fichet, D. Teyssie, S. Cantin, *Langmuir* **2013**, *29*, 9499.
[53] H. S. Lim, J. T. Han, D. Kwak, M. Jin, K. Cho, *J. Am. Chem. Soc.* **2006**, *128*, 14458.
[54] M. Callies, D. Quéré, *Soft Matter* **2005**, *1*, 55.
[55] G. d. Crevoisier, *Science* **1999**, *285*, 1246.
[56] B. Xin, J. Hao, *Chem. Soc. Rev.* **2010**, *39*, 769.
[57] D. Tian, Y. Song, L. Jiang, *Chem. Soc. Rev.* **2013**, *42*, 5184.


© 2016 WILEY-VCH Verlag GmbH & Co. KGaA, Weinheim